Student Conference Proceedings
Vol 2, No 1, 2026, Article ID 2559, 4 Pages

Student Conference Lübeck

Proceedings Article

Optimizing Detector Location in Prompt Gamma Timing for Stopping Power and Range Estimations in Proton Therapy.

Zahra Aliyeva [a,*] · Magdalena Rafecas [b] · Julius Werner [b,*]

[a] Study program Biomedical Engineering, Luebeck University of Applied Sciences, Lübeck, Germany
[b] Institute of Medical Engineering, Universität zu Lübeck, Lübeck, Germany
[*] Corresponding author, email: zahra.aliyeva@stud.th-luebeck.de, email: friedemann.werner@uni-luebeck.de

Received 09 April 2026; Accepted 04 September 2026; Published online 07 September 2026

Abstract

Proton therapy for tumour treatment exploits the characteristic energy-deposition pattern of protons in tissue to spare surrounding healthy structures; however, uncertainties in particle range arising from imperfect stopping-power estimation and patient positioning require safety margins. Prompt Gamma Timing (PGT) addresses this gap by measuring the arrival times of prompt gammas in external detectors and correlating them with the passage of primary protons. In this way, PGT enables in vivo range verification. In this work, a Python framework that integrates an analytical PGT model was developed to optimize detector locations for the MERLINO detection concept. The algorithm iteratively identifies the least useful detectors, proposes new positions and evaluates reconstruction metrics over many configurations, yielding layouts with reduced mean relative error from iteration to iteration. This optimization framework provides the first integration of an analytical PGT model into an automated detector-layout optimization tool within the PROSIT project, enabling systematic studies of MERLINO-like detector configurations.

I. Introduction

Charged particle therapy (CPT) with protons or heavier ions makes use of their particular depth–dose distribution in matter, with a sharp peak at the end of their range, the Bragg peak. The latter enables high tumor dose while sparing healthy tissue [1]. In current clinical workflows, the position of the Bragg peak is predicted from X-ray CT images that are converted into maps of proton stopping power (i.e. the energy loss of protons per unit path length in each tissue), and treatment plans include margins to account for residual uncertainties in this prediction, as well as in patient setup and anatomical changes [2].

Within the DFG-funded project *Proton Stopping power estimation in Ion Therapy* (PROSIT), an independent measurement of the stopping power is pursued based on secondary radiation produced during treatment. Specifically, the time between primary particles entering the patient and prompt gamma (PG) photons interacting in detectors around the patient is measured. The PGT technique uses the fact that PG emission is almost instantaneous after nuclear interactions along the particle path, so that the spatiotemporal PG emission distribution is closely linked to the proton transport through the patient [3], [4]. The spatiotemporal reconstruction of PG emissions enables verification of the stopping-power distribution used in treatment planning, rather than replacing CT-based stopping-power estimation.

The performance of a PGT system depends critically on the configuration of the PG detectors, including their number, locations, geometry and material. This study focuses on optimizing detector locations for the exist-

ing MERLINO prototype [5] and preparing the software infrastructure needed to study the required number of detectors. To this aim, we developed a Python-based optimization framework that interfaces with the analytical PGT model from PROSIT, searches over admissible detector positions defined by geometric and clinical constraints, and implements robust stopping criteria and logging to enable systematic detector-layout studies. The main contribution of this work is an automated detector-layout optimization framework that provides a unified software environment for varying and assessing detector configurations, rather than manually testing individual layouts.

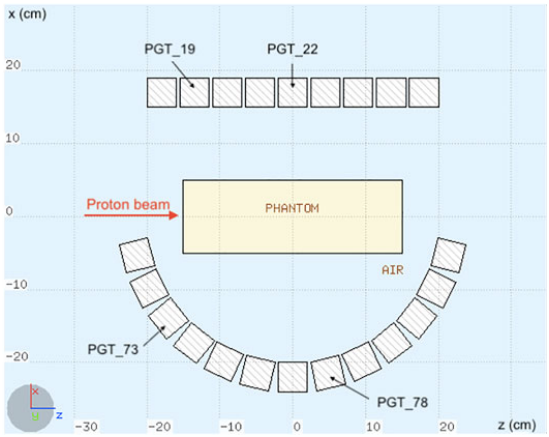

Figure 1: Schematic of the simulated PGT setup: proton beam along z direction in a homogeneous PMMA (polymethyl methacrylate) phantom, and a total of 110 $LaBr_3$:Ce detectors placed asymmetrically around the target in 5 rows along the y axis as simulated in previous works (central section shown) (adapted from Ferrero et al. [5] under license CC BY.)

II. Methods and materials

This section summarizes the PGT model and the optimization framework used.

II.I. PGT principle in PROSIT

In CPT, prompt gamma photons with energies up to a few MeV are produced in inelastic nuclear interactions of the treatment beam with patient tissue and beamline components [6], [7]. Their emission is essentially instantaneous, so the time difference between a reference signal for the arrival of the primary protons and the detection of a PG photon encodes information on the emission position along the beam path [3]. This time-of-flight (TOF) principle forms the basis of PGT for range verification.

The dedicated PGT framework combines Monte Carlo (MC) simulations of the spatiotemporal PG emission distribution with an analytical model that maps this emission to detector time spectra for a given patient geometry and detector configuration [8]. A schematic of the simulated PGT setup used in this study is shown in Fig. 1.

II.II. Detector configurations and evaluation

The optimization framework is based on a MERLINO-like detector design consisting of fixed-size $LaBr_3$ crystals with a (3.81 cm×3.81 cm) length cross - section. The optimization acts only on the two-dimensional positions and orientations of detectors, while keeping their size, shape and material fixed.

In the optimization process, the detector positions are varied within a clinically admissible region around the patient. Each configuration is defined by the Cartesian coordinates (x, y, z) of each detector centre in the treatment-room coordinate system [9]. In the present 2D study, the detectors are confined to the x–z plane. Detectors are excluded from the forbidden region ("red zone") comprising the beam path and patient volume (see in Fig. 2). Candidate positions are sampled only from the admissible region $15\,\text{cm} \le x \le 40\,\text{cm}$, $-50\,\text{cm} \le z \le 50\,\text{cm}$, corresponding to realistic locations outside the patient.

For a given configuration, the analytical PGT model provides detector time spectra based on the beams and phantom described in[9]. From these spectra, the stopping power and the range are reconstructed using in-house developed algorithms, and the reconstruction quality is quantified through primarily the mean relative error (MRE) defined as the voxel-wise average relative difference average of the relative difference between reconstructed and reference stopping power over the region of interest [9]. Additional figures of merit (FOMs), namely range error and Stopping Power Ratio error (SPR), were monitored to verify that the optimization consistently improves reconstruction performance across multiple metrics. The SPR evaluates the relative error of reconstructed SPR along the beam path, while the range error quantifies the residual mismatch between reconstructed and reference Bragg-peak positions [9].

II.III. Simulation data and preprocessing

Representative test cases were generated within the PROSIT framework using FLUKA Monte Carlo simulations [9]. For each detector configuration and beam setting, monoenergetic proton pencil beams (energies between approximately 60 MeV and 220 MeV) impinge on a homogeneous PMMA phantom, and the spatiotemporal distribution of prompt gamma emission is simulated in the full 20 detector geometry. This output is then processed by existing C++ codes that bin the simulated events in time, energy and emission position and write

10.18416/SCP.2026.2559

histograms and geometry information to text files read by the Python framework.

II.IV. Optimization algorithm and implementation

The implemented algorithm follows a local search scheme in which detector configurations are iteratively modified and evaluated with the analytical PGT model. Its control flow is summarised in two main components:

1. an loop of up to 200 iterations that proposes new detector configurations, and
2. an acceptance rule that updates the current configuration only if the FOM improves.

The procedure is 'evolution-inspired' in the sense that, in each iteration, only small random changes to the current configuration are proposed, and configurations with improved figures of merit are retained. Unlike full evolutionary algorithms or genetic algorithms, this scheme does not maintain a population of candidate solutions, but focuses on a single incumbent configuration that is locally improved.

In each iteration, the code identifies the three least useful (TLU) detectors by temporarily removing each detector and recording the resulting change in FOM. Detectors whose removal causes the smallest FOM degradation define the TLU set. New positions for the TLU detectors are then randomly sampled from the continuous admissible region, yielding one candidate configuration per iteration. A candidate configuration is accepted as the new best layout only if its average MRE across all 17 beam energies is lower than that of the current best configuration; otherwise, the previous configuration is kept. All FOMs used here are defined such that lower values indicate better reconstruction performance. In the present study, the optimization is initialized from a randomstarting configuration; different starting layouts could in principle lead to different final arrangements and performance. In this study, the optimization was run once for 200 iterations using a single fixed random seed; it reports the best configuration found during this run. Because the reconstruction is computationally expensive, the underlying C++ codes are executed in parallel on a multi-core system. Optimization is initialized with a MERLINO-based configuration with 20 $LaBr_3$ detectors, whose FOMs are evaluated using the analytical model and the automatic scenario-based hyperparameter optimization and FOMs introduced in [9].

III. Results and Discussion

After 73 iterations, no further candidate configuration yielded a lower mean relative error, so configuration 73 was reported as the best one found within the tested position space. This result was obtained using a fixed random seed; future work will investigate multiple seeds to assess robustness. A single optimization run with up to 200 configurations is computationally demanding and currently takes 17 hours on a 96-core CPU, so within this work only one fixed random seed was studied systematically; future work will perform several runs with different seeds to assess robustness and identify common features of good detector configurations.

Figure 2 shows the initial and final detector layouts. Within the admissible region beside the patient (Section II), several detectors move compared to the initial layout. The optimised configuration shows improved coverage of the distal part of the beam path and a wider spread in lateral viewing angles. This arrangement allows detectors to capture complementary timing information from different perspectives for improved emission reconstruction[5]. A wider spread of lateral viewing angles means that detectors observe prompt gamma photons from different directions and path lengths, potentially improving complementary time-of-flight information and geometric coverage so that stopping power and range can be reconstructed more accurately.

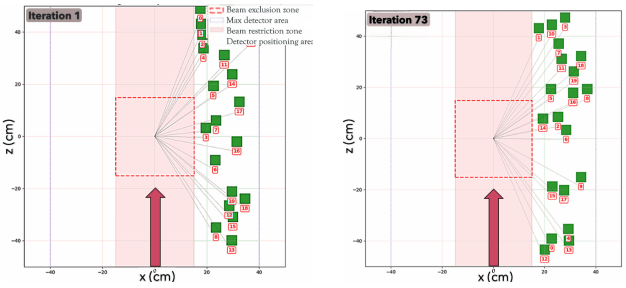

(a) (b)

Figure 2: Detector positions before (a) and after (b) optimization. In both panels the arrow indicates the proton beam direction.

Figure 3 shows the evolution of the three figures of merit over accepted configurations: the MRE, which serves as the primary optimization target, and the SPR and range error, which are monitored as secondary quantities to ensure that improvements in MRE do not come at the expense of range accuracy or SPR performance. The most important quantity is the MRE of the reconstructed stopping power. Smaller values therefore indicate a better global match between reconstructed and reference distributions. Starting from tested initial layouts, the MRE improves quickly starting from the first iterations. Minor fluctuations are observed but remain below 10% for the later configurations. All three metrics (MRE, SPR, range error) improve overall, even though only the MRE was explicitely considered in the optimization. The final configuration achieves acceptable performance (MRE:

10.18416/SCP.2026.2559

6%, SPR: 5%), demonstrating that the optimization approach works.

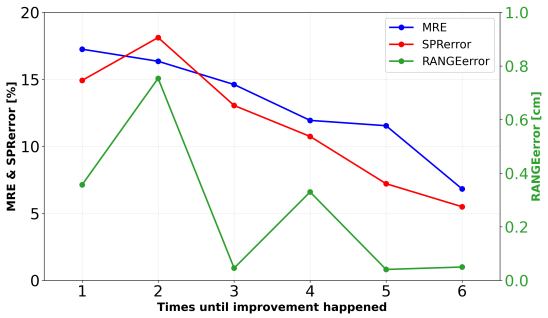

Figure 3: Evolution of error metrics over accepted detector configurations. The plotted FOM values start from the first accepted improvement after the initial random configuration.

It is not yet known if configuration 73 is the best possible arrangement or just a good local solution.

To build confidence, the algorithm should be run multiple times with different random starting points. This will show whether it consistently finds similar detector arrangements (suggesting robustness) or finds very different ones (suggesting a complex optimization landscape). Testing small changes to configuration 73 will reveal how sensitive the solution is to precise positioning—critical for clinical implementation. Extended runs with different algorithm parameters may also find better configurations. More sophisticated optimization techniques, such as simulated annealing, genetic algorithms, or particle swarm optimization, could in principle explore the configuration space more globally. Evaluating such methods within the PROSIT framework is left for future work.

IV. Conclusion

Using an analytical model of PGT, a Python framework was developed to search for improved detector locations for a MERLINO-based PGT system. The final configuration showed reduced MRE compared to the initial layout and fulfils the stopping criteria implemented in the code.

Future work will test the robustness of the method by starting optimizations from different initial detector configurations. Although attenuation of prompt gamma photons by surrounding detectors and other materials is implemented in the model, it was deactivated for the present tests. Further extensions include tighter coupling to realistic patient geometries and beam settings, and explicit variation of detector numbers. This will enable systematic studies of layouts balancing information content, hardware complexity, and clinical feasibility, bringing PGT-based stopping-power estimation closer to practical implementation in charged particle therapy.

Acknowledgments

This work was partially supported by the German Research Foundation (DFG) by Grant No. 51658731 3 (PROSIT) and supervised by the Institute of Medical Engineering, Universität zu Lübeck. The authors thank Sophie Lazenby, The University of Manchester, for proofreading.

Author's statement

Conflict of interest: The author states no conflict of interest.

References

[1] A. J. Lomax. Myths and realities of range uncertainty. *British Journal of Radiology*, 93(1107):20190582, 2020, doi:10.1259/bjr.20190582.

[2] R. Liu *et al.* Dosimetric impact of range uncertainty in passive scattering proton therapy. *Journal of Applied Clinical Medical Physics*, 22(3):6–14, 2021, doi:10.1002/acm2.13179.

[3] C. Golnik, F. Hueso-González, A. Müller, P. Dendooven, W. Enghardt, F. Fine, *et al.* Range assessment in particle therapy based on prompt γ-ray timing measurements. *Physics in Medicine and Biology*, 59(18):5399–5422, 2014, doi:10.1088/0031-9155/59/18/5399.

[4] T. Werner, J. Berthold, F. Hueso-González, T. Kögler, J. Petzoldt, K. Römer, *et al.* Processing of prompt gamma-ray timing data for proton range measurements at a clinical beam delivery. *Physics in Medicine and Biology*, 64(10):105023, 2019, doi:10.1088/1361-6560/ab176d.

[5] V. Ferrero, J. Werner, P. Cerello, E. Fiorina, A. Vignati, F. Pennazio, and M. Rafecas. Estimating the stopping power distribution during proton therapy: A proof of concept. *Frontiers in Physics*, 10:971767, 2022, doi:10.3389/fphy.2022.971767.

[6] B.-W. Cheon and C. H. Min. Prompt gamma imaging system in particle therapy: A mini-review. *Frontiers in Physics*, 12:1356572, 2024, doi:10.3389/fphy.2024.1356572.

[7] J. Krimmer, D. Dauvergne, J. M. Létang, and É. Testa. Prompt-gamma monitoring in hadrontherapy: A review. *Nuclear Instruments and Methods in Physics Research Section A: Accelerators, Spectrometers, Detectors and Associated Equipment*, 878:58–73, 2018, doi:10.1016/j.nima.2017.07.063.

[8] J. Werner, V. Ferrero, J. Roser, J. Kasprzak, F. Pennazio, M. Rafecas, *et al.*, Analytical model of prompt gamma timing for spatiotemporal reconstruction, 2026. doi:10.1088/1361-6560/ae54ff.

[9] J. Werner, V. Ferrero, F. Pennazio, P. Cerello, E. Fiorina, J. Kasprzak, and M. Rafecas. Stopping power and range estimations in proton therapy using prompt gamma timing: Motion models and automated parameter optimization. *Physics in Medicine and Biology*, 69(14):14NT02, 2024, doi:10.1088/1361-6560/ad5d4b.